

## Photon-induced defects and dynamics of photogenerated carriers in Cu(In, Ga)Se<sub>2</sub> thin film solar cells

Yunae Cho<sup>a</sup>, Jiseon Hwang<sup>b</sup>, Inyoung Jeong<sup>b</sup>, Jihye Gwak<sup>c,d</sup>, Jae Ho Yun<sup>b,d</sup>, Kihwan Kim<sup>b,d,\*\*</sup>, William Jo<sup>a,\*</sup>

<sup>a</sup> Department of Physics, Ewha Womans University, Seoul, 03760, Republic of Korea

<sup>b</sup> Photovoltaics Laboratory, Korea Institute of Energy Research (KIER), Daejeon, 34129, Republic of Korea

<sup>c</sup> New and Renewable Energy Institute, Korea Institute of Energy Research, Daejeon, 34129, Republic of Korea

<sup>d</sup> Renewable Energy Engineering, University of Science and Technology (UST), Daejeon, 34113, Republic of Korea



### ARTICLE INFO

#### Keywords:

Cu(In,Ga)Se<sub>2</sub> thin film solar cells  
Photo-induced defect  
J-V distortion  
Persistent photo-capacitance  
Band structures

### ABSTRACT

A detailed understanding of charge-carrier behavior could provide new avenues to improve the performance of the solar cell by enhancing the active materials and electronic properties. In the present work, the transport mechanism of photogenerated carriers in Cu(In,Ga)Se<sub>2</sub> or CIGS-based solar cells is investigated by analysis of the temperature-dependent current density-voltage (*J-V*) curves obtained under various illumination (i.e., dark, AM 1.5G, 650 nm, and 405 nm). The results demonstrate that *J-V* curve distortion, termed the “roll-over” effect, is significantly correlated with the illumination wavelength and, more importantly, is strongly associated with the persistent characteristics of the CIGS solar cell. In addition, the nature of the photo-induced defects and their influence on the transport mechanism of the photogenerated carriers were investigated via deep level capacitance profiling (DLCP) and admittance spectroscopy (AS) under various illumination conditions. The photo-capacitance results indicate distinct spatial distributions and persistent behaviors depending upon the illumination wavelength. Based on the findings in this work, the origin of the non-ideal *J-V* behavior in the CIGS solar cell is explained, and the spatial defect distribution and illumination wavelength sensitivity are discussed.

### 1. Introduction

Recently, Cu(In,Ga)Se<sub>2</sub> or CIGS-based thin film solar cells have achieved efficiencies in excess of 23%. Thus, in-depth physical analyses of the material and the devices constructed therefrom are becoming increasingly important for continued progress [1,2]. To enhance the performance of solar cells, various properties based on the electronic band structure have been investigated. These include the current density-voltage (*J-V*) characteristics based on the circuit and device, the diode qualities [3], and the series and shunt resistances [4,5]. Additionally, capacitance analysis for the p-n junction has been performed, including examination of the charge density and frequency-dependent spatial distribution and dynamics of charge carriers in relation to the defect states [6–8]. Further, as a function of temperature and illumination, the transport process [3,9], persistent behavior [10–16], and intrinsic material properties such as the band structure [4,17] have been examined for CIGS solar cells. While individual analyses of these solar

cells have been thoroughly performed, continued progress in this field requires a comprehensive understanding of the device characteristics obtained via direct observation.

Compared with the intrinsic charge-carrier transport properties in the dark, illumination generates excess carriers that experience distinct transport mechanisms. This can be verified by the lack of overlap between the dark and photo current density-voltage curves. The voltage-dependence of the light current density,  $J_{\text{light}}$ , of CIGS solar cells rarely follows the relationship with the short circuit current density,  $J_{\text{SC}}$ , given by Eq. (1) [18]:

$$J_{\text{light}}(V) = J_{\text{dark}}(V) + J_{\text{SC}} \quad (1)$$

Rather, the voltage-dependence of  $J_{\text{light}}$  is related to the photo current density,  $J_{\text{ph}}$ , in accordance with Eq. (2):

$$J_{\text{light}}(V) = J_{\text{dark}}(V) + J_{\text{ph}}(V) \quad (2)$$

The voltage dependence can be seen as a distortion of the *J-V* curves,

\* Corresponding author.

\*\* Corresponding author.

E-mail addresses: [kimkh@kier.re.kr](mailto:kimkh@kier.re.kr) (K. Kim), [wmjo@ewha.ac.kr](mailto:wmjo@ewha.ac.kr) (W. Jo).

such as a rollover or a red kink. The rollover indicates current saturation at a forward bias which may be due to the back contact barrier [19–21], the defect states [10,22], or a positive conduction band offset [16,22]. The red kink occurs in the third or fourth quadrant of the *J-V* curve and may be due to the positive conduction band offset [22], a thin p+ layer at the absorber front surface, or a conduction band gradient [2]. Clearly, the specific origin of the *J-V* distortion remains a controversial issue. Nevertheless, the *J-V* distortion has been shown to be related to the photogenerated current, and this illumination effect has persistent properties and is dependent on the various wavelengths of light [10,11, 23–25]. The persistent properties lead to the gradual decay of the photo-generated charge carrier effects over time, with one such property manifesting itself as a long photoconductivity relaxation time after switching the light off. This behavior is hypothesized to originate from excess electrons trapped in deep defects, where either large lattice relaxation or potential fluctuations hinder re-emission [26]. The light soaking effect has been suggested to reduce distortion [14,16,27]. However, while the majority of studies have examined the residual effect of illumination after switching the light off, actual solar cells operate under illumination and, hence, an understanding of the device properties in the light-active state is crucial for enhancing solar cell performance.

Hence, the present study examines the photo-induced defects in CIGS solar cells and suggests a possible transport mechanism. Device characterization is performed under various illumination conditions (i.e., dark, AM 1.5G, 405 nm, and 650 nm) and various temperatures. The spatial defect distribution and carrier dynamics obtained from the photocurrent and photo-capacitance measurements indicate how photogenerated charge carriers are transported in the device and result in *J-V* distortions such as roll-over and kink. The origin of the wavelength-dependent *J-V* distortion is examined by characterizing the persistent behavior via analysis of the band structure. A novel interpretation of the photocarrier dynamics is suggested to explain the *J-V* characteristics of real devices and to offer a way to realize highly efficient devices.

## 2. Experimental section

### 2.1. Fabrication of CIGS solar cells

A 0.7 μm-thick Mo back contact was grown on a soda-lime glass (SLG) substrate from a 99.99%-pure Mo target using a pulsed DC magnetron sputtering system. The CIGS absorber layers were prepared by evaporation of In, Ga, Cu, and Se in the following three-stages: (i) In, Ga, and Se were evaporated on the substrates at 350 °C to form an (In, Ga)<sub>2</sub>Se<sub>3</sub> layer with a thickness of 1 μm; (ii) Cu and Se were evaporated and reacted directly with the (In, Ga)<sub>2</sub>Se<sub>3</sub> layer at ~550 °C to form a Cu-rich CIGS film, and (iii) In, Ga, and Se were evaporated on the CIGS layer to convert the film to a Cu-poor CIGS composition. To complete the CIGS solar cells, CdS buffer layers (~50 nm) were deposited onto the CIGS films via chemical bath deposition. Then, intrinsic ZnO (~50 nm) and indium tin oxide (~150 nm) window layers were deposited via radio frequency (RF) sputtering. Finally, Al electrodes were deposited by e-beam evaporation. The Ga/(In + Ga) ratio of the obtained film is indicated in the scanning electron microscope (SEM) image in Fig. S1 of the Supplementary Material, and is comparable to previously-published data for a highly-efficient CIGS solar cell [28].

### 2.2. Optical and electrical characterization

The *J-V* characteristics of the devices were measured using a source meter (Keithley 2450) under irradiation by simulated AM 1.5G sunlight and laser modules with 650-nm and 405-nm wavelength emission (Dot beam laser, Laser Lab). The intensities of the laser modules were ~30 mW/cm<sup>2</sup>, as measured using a power meter (Pronto-Si, Gentec-EO). Before reaching the CIGS, the intensities of the 650 and 405 nm lights were attenuated by 86.0 and 63.9%, respectively, by passage through an

ITO/i-ZnO/CdS structure, as indicated by the transmittance and external quantum efficiency (EQE) in Fig. S2. From the previously-published absorption coefficient data for the CIGS thin film [29], the penetration depths of the 650-nm (1.91 eV) light and the 405-nm (3.06 eV) light were ~170 nm and 30 nm, respectively. Thus, the 650 nm photons appeared to be mostly absorbed in the CIGS bulk, while the 405 nm photons were mostly absorbed in the CdS/CIGS interface. Admittance spectroscopy (AS) was performed using a varying AC frequency of 100 Hz to 1 MHz, and drive-level capacitance profiling (DLCP) was performed at a frequency of 10 KHz. Both the AS and DLCP measurements were performed using an LCR meter (Agilent 4284 A, Keysight) with a temperature-controlled probe stage (LTSE350-P, Linkam) to vary the temperature between 80 and 300 K in steps of 10 K. Before illumination, the sample was held in the dark for over 12 h at 300 K prior to cooling down to 100 K. Transient capacitance measurements were then performed at 10 kHz at both 100 and 300 K during 200 s of illumination under 650 and 405 nm light. In addition, measurements were made before the lights were turned on, and continued for an additional 300 s after the lights were turned off. Before illumination, the CIGS solar cells were rested under dark conditions for 30 min at 40 °C to deactivate any persistent behaviors in the device.

## 3. Results and discussion

The temperature dependent *J-V* characteristics of the CIGS solar cells were investigated from 100 to 300 K at 20 K intervals under AM1.5G, superimposed AM1.5G and 405 nm light (hereafter, AM1.5G+405), 650 nm, 405 nm, and superimposed 650 nm and 405 nm light (hereafter, 650 + 405). The results are presented in Fig. 1, and the related device characteristics are given in Table 1. Distortion in the temperature dependent *J-V* curves of the solar cells under AM 1.5G light is clearly evident in Fig. 1a and is primarily due to the roll-over effect observed at low temperature. However, this distortion disappears under AM 1.5G+405 illumination, as shown in Fig. 1b. To investigate the spectral dependence of the *J-V* characteristics under illumination, the device was also separately subjected to 650 and 405 nm light (Fig. 1c and d). Here, severe distortion is observed under 650 nm light (Fig. 1c) but not under the 405 nm light (Fig. 1d). In addition, the distortion observed under 650 nm light is eliminated by illumination under superimposed 650 and 405 nm light, as shown in Fig. 1e. Although the efficiency (Eff.), open-circuit voltage ( $V_{OC}$ ), and short-circuit current density ( $J_{SC}$ ) values could not be directly compared due to the various illuminations, the results in Table 1 indicate that the fill factor (FF) values exhibit a significant dependence on the type of illumination. This dependence is particularly noticeable at low temperature, where FF values of 67.0%, 42.18%, and 78.55% are obtained under AM1.5G, 650 nm, and 405 nm illumination, respectively (see Fig. 1).

As demonstrated in the Experimental section, the 405 nm light only reaches ~30 nm into the CIGS absorber layer (including the CdS/CIGS interface); hence, the disappearance of the distortion and the improved FF when this wavelength is superimposed on the 650 nm illumination can be attributed to the effect of the 405 nm wavelength upon the CdS/CIGS interface region. The mechanism of this effect can be attributed to residual conductivity caused by illumination under the short wavelength light [27], as demonstrated by the *J-V* curves obtained at low temperature (100 K) in Fig. 2. Here, the distortion under 650 nm light (red solid line) disappears when the 650 nm light is switched off and the sample is immediately illuminated for 10 min under 405 nm light (blue solid line). Further, the distortion does not reappear upon subsequent illumination with 650 nm light after switching off the 405 nm light (solid purple line). These results suggest that the persistent *J-V* characteristics of the CIGS solar cells are associated with the roll-over effect and are sensitive to blue light illumination (405 nm laser in the present work).

For a more detailed investigation, the  $V_{OC}$  values of the CIGS solar cells under the various illuminations are plotted as a function of

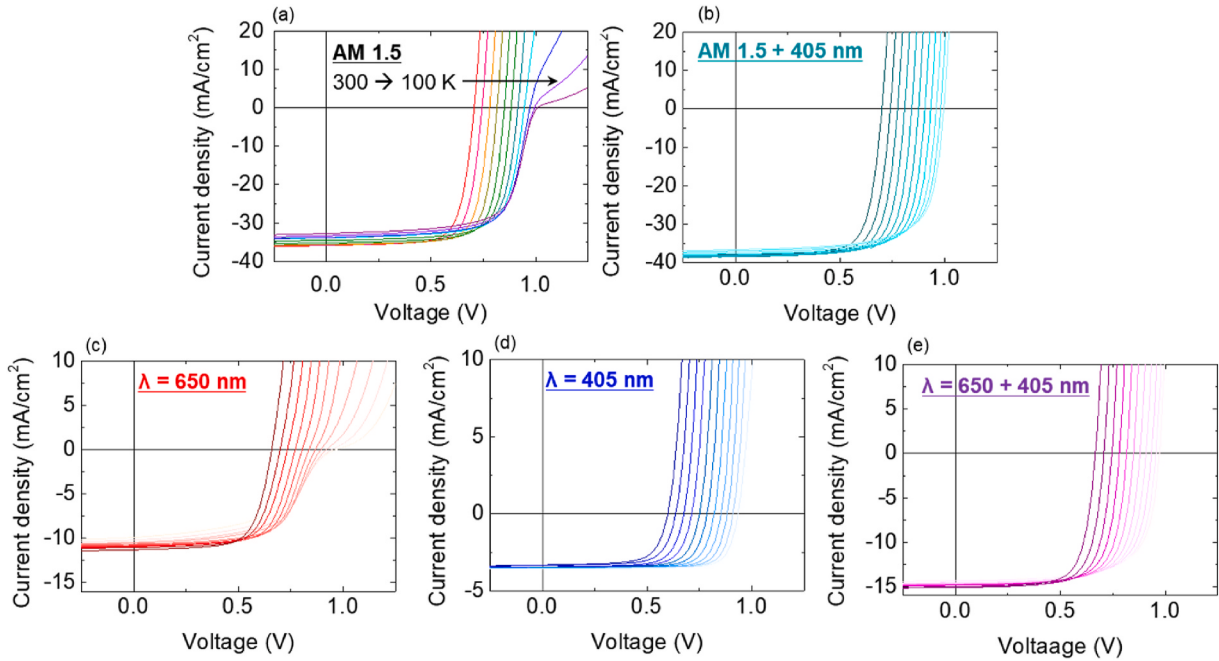


**Fig. 1.**  $J\text{-}V$  characteristics of the cell under (a) AM1.5, (b) AM1.5 + 405 nm, (c) 650 nm, (d) 405 nm, and (e) 650 + 405 nm illumination as a function of temperature from 80 to 300 K.

**Table 1**

Solar cell performance at room temperature.

Eff. (%)	$V_{OC}$ (V)	$J_{SC}$ (mA/cm <sup>2</sup> )	FF (%)
16.8	0.70	32.8	73.1

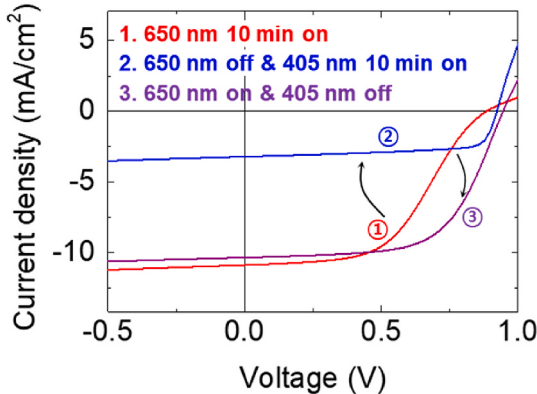


**Fig. 2.**  $J\text{-}V$  curves with the observed persistent behavior under 650 and 405 nm light.

temperature in Fig. 3. Here, a linear correlation between  $V_{OC}$  and  $T$  is observed under both illumination conditions at temperatures close to 200 K. Among the various light sources, the AM1.5G illumination gives the highest  $V_{OC}$  values, followed by the separate 650 nm and 405 nm light, respectively, over the entire investigated temperature range. However, whereas the  $V_{OC}$  begins to saturate at temperatures of less than 200 K under the 650 nm illumination, saturation begins at an even lower temperature of  $\sim 160$  K under the AM1.5G and 405 nm light. As shown in Fig S3, when the diode ideality factor ( $A$ ) is temperature independent, the activation energy,  $E_a$ , is determined by the dominant carrier transport process and is given by the extrapolation of the plot of  $V_{OC}$  vs.  $T$  to  $T = 0$  K, in accordance with Eq. (3) [2,30]:

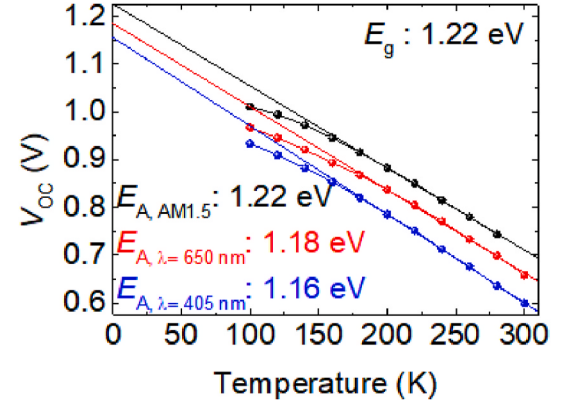


**Fig. 3.** Temperature dependence of the  $V_{OC}$  under the illumination; AM1.5 (black), 650 nm (red), and 405 nm (blue). The bandgap ( $E_g$ ) of the tested CIGS solar cell was estimated by means of the external quantum efficiency. (For interpretation of the references to colour in this figure legend, the reader is referred to the Web version of this article.)

$$V_{OC} = \frac{E_a}{q} - \frac{Ak_B T}{q} \ln \left( \frac{J_{00}}{J_{SC}} \right), \quad (3)$$

where  $q$  is the electron charge,  $k_B$  is Boltzmann's constant,  $T$  is the temperature, and  $J_{00}$  is the pre-factor of the saturation current density. The results in Fig. 3 indicate that the  $E_a$  under AM 1.5G illumination and 650 nm light are close to the bandgap energy  $E_g$ , thus suggesting that the recombination process occurs primarily in the bulk. Under the 405 nm illumination, however, the  $E_a$  value is significantly lower than  $E_g$ , thus indicating that interface recombination is insignificant at this wavelength [4].

Taken together, the above  $J\text{-}V$  and  $V_{OC}$  results suggest that the wavelength- and temperature-dependent  $J\text{-}V$  distortion can be associated with the main recombination process. As shown in Fig. 4, this correlation is further clarified via the drive-level capacitance profiling (DLCP) technique to obtain the spatial distribution of the drive level

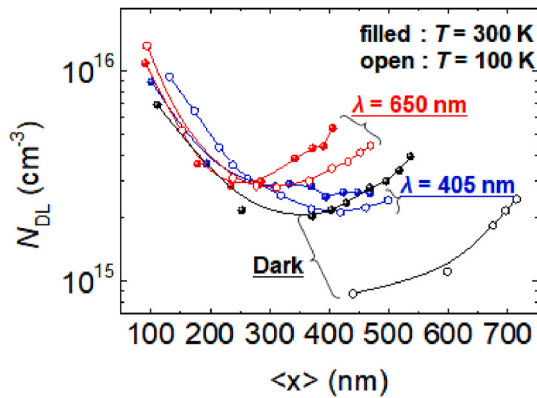


**Fig. 4.** DLCP measurement of CIGS thin film solar cells in the dark and under illumination with temperature; 300 K (filled circles) and 100 K (open circles).

defect density ( $N_{\text{DL}}$ ) for each cell, which consists of the sum of the net charge density ( $N_p$ ), the bulk defect density ( $N_b$ ), and the photo-generated carrier density ( $N_{\text{ph}}$ ). The DLCP technique focuses on the nonlinear terms of charge response from the ac voltage according to Eq. (4):

$$\frac{dQ}{dV} = C_0 + C_1 dV + C_2 (dV)^2 + \dots \quad (4)$$

According to Heath et al. [6], the  $N_{\text{DL}}$  at the position  $\langle x \rangle$  is then determined using Eqns. (5) and (6):

$$\langle x \rangle = \varepsilon S / C_0, \quad (5)$$

$$N_{\text{DL}} \equiv -\frac{C_0^3}{2q\varepsilon S^2 C_1}, \quad (6)$$

where  $q$  is the charge,  $V$  is the voltage,  $C_{0,1,2}$  is the relevant coefficient of capacitance,  $S$  is the area, and  $\varepsilon$  is the permittivity. As the obtained  $N_{\text{DL}}$  values incorporate the contributions of both  $N_p$  and  $N_b$  [6], this can be compared to the sum of  $N_p$  and  $N_b$  in the dark in order to separate out the ‘pure’  $N_{\text{ph}}$  values; i.e.,  $N_{\text{ph}} = N_{\text{DL}}(\text{illumination}) - N_{\text{DL}}(\text{dark})$ . From the results, the  $N_{\text{ph}}$  under 650 nm light was found to increase by 1.5 times compared to that under 405 nm light as shown in Table 2, and the  $J_{\text{ph}}$  under 650 nm light increased by 3 times compared to that under 405 nm light. Thus, although the increasing degree is different, the increase in  $N_{\text{ph}}$  under 650 nm illumination compared to that under 405 nm illumination is consistent with the increase in  $J_{\text{ph}}$ . The  $N_b$  values decreased under each type of illumination to become smaller than that under dark conditions, with the effect under 650 nm illumination being especially evident. This reduction in the  $N_b$  can be attributed to charge compensation of the bulk defect states by the photogenerated carriers at 650 and 405 nm, as has been generally observed in previous studies [31]. Thus, differences in the  $N_{\text{DL}}$  values were noted in the spatial distribution depending on the light conditions. In comparison to the  $N_{\text{DL}}$  in the dark, the  $N_{\text{DL}}$  under the 650 nm light with a long penetration depth in the CIGS absorber exhibited a greater effect on the bulk than that under the 405 nm light with a short penetration depth. In terms of the spatial distribution, it should be noted that the  $N_{\text{DL}}$  at the interface is larger than that in the bulk at low temperature under illumination with either 650 or

405 nm whereas, in the dark, the  $N_p$  is less at low temperature than at high temperature over the entire distribution.

The photogenerated charge carrier transport mechanism at low temperature is different from the thermionic charge carrier transport phenomenon, which several previous studies have relied upon to a large degree. Hence, frequency-dependent capacitance profiles were obtained via admittance spectroscopy (AS) at various temperatures and under various illumination conditions (dark, 405 nm, and 650 nm) to examine the dynamics of photogenerated carrier exchange via defect states [2], as shown in Fig. 5. Thus, in the dark, the CIGS solar cells exhibit the typical step-shaped admittance spectra of Fig. 5a. In previous studies, the decreasing capacitance at low temperature has generally been attributed to freezeout of most of the charge carriers due to a reduction in the thermionic energy [2,5,32]. However, although the general trends of the AS spectra obtained under 650 nm illumination in the present work (Fig. 5b) follow that of typical AS spectra, their shapes do not exhibit extreme sensitivity to temperature. By contrast, the spectra obtained under 405 nm light (Fig. 5c) exhibit an unexpected reversal in the temperature dependence of the capacitance, as has been previously reported by Rockett et al. [33]. This yielded a new interpretation for the transport process, as described in detail later in the present section.

The density of defect states (DOS) were extracted from the AS data according to Eqns. (7) and (8) [34]:

$$\omega_0 = 2N_{C,V}v_{\text{th}}\sigma_{e,h}\exp\left(-\frac{E_T}{kT}\right) = \xi_0 T^2 \exp\left(-\frac{E_T}{kT}\right) \quad (7)$$

$$E_{\omega} = kT \ln\left(\frac{\xi_0 T^2}{\omega}\right) \quad (8)$$

where  $\omega_0$  is the inflection frequency of the capacitance step,  $N_{C,V}$  is the effective density of state at the conduction band minimum and valence band maximum,  $v_{\text{th}}$  is the thermal velocity,  $\sigma_{e,h}$  is the capture cross-section of electrons and holes,  $E_T$  is the energy-level of the defect state,  $k$  is Boltzmann’s constant,  $T$  is the temperature in Kelvins. The trap density of states,  $N_t$ , is plotted as a function of the  $E_{\omega}$  value from equation (8) according to Eq. (9):

$$N_t(E_{\omega}) = -\frac{U_d}{qw} \frac{dC}{d\omega} \frac{\omega}{kT} \quad (9)$$

where  $U_d$  is the built-in potential,  $q$  is the electron charge, and  $w$  is the depletion width. The results for the cell under the three illumination conditions are plotted in Fig. 5d-f, thus indicating that defect states present at 150 and 100 meV in the dark are compensated under each of the two illumination conditions. In addition, new shallow defect states are observed at 100 and 50 meV under the 650 nm illumination, and at 20 meV under the 405 nm illumination.

Observing the response of the solar cells to excitation under 650 and 405 nm wavelength light allows an examination of the photo-capacitance dynamics with respect to temperature and illumination wavelength, as shown in Fig. 6 and Table 3. Here, the time transient capacitance profiles are seen to react differently to each type of illumination. Thus, at 300 K, a fast initial rise (i.e., an overshoot) is observed under the 650 nm illumination when the light source is switched on, whereas a slower rise occurs under the 405 nm illumination. This photo-capacitance overshoot has been previously interpreted in terms of strong trap-mediated recombination due to faster charge capture relative to charge emission. Thus, the recombination rate has generally been observed to increase with increasing charge density under illumination [35, 36]. The photogenerated charge carriers under 650 nm light are hypothesized to undergo trap-mediated recombination, while a strong build-up of trapped carriers is expected to occur under 405 nm light. When the light is switched off, persistent photo-capacitance tails are observed for each of the two illuminations (Fig. 6), in agreement with previous studies [11,15,23,25]. Further, the extent of the persistent photo-capacitance is significantly larger under blue (405 nm)

**Table 2**  
DLCP results of the CIGS solar cells derived from Fig. 3.

Wavelength (nm)	Net charge density, $N_p$ ( $\text{cm}^{-3}$ )	Bulk defect density, $N_b$ ( $\text{cm}^{-3}$ )	Photogenerated carrier density, $N_{\text{ph}}$ ( $\text{cm}^{-3}$ )
Dark	$8.74 \times 10^{14}$	$1.17 \times 10^{15}$	
405	$2.13 \times 10^{15}$	$3.97 \times 10^{14}$	$1.26 \times 10^{15}$
650	$2.80 \times 10^{15}$	$5.21 \times 10^{13}$	$1.92 \times 10^{15}$

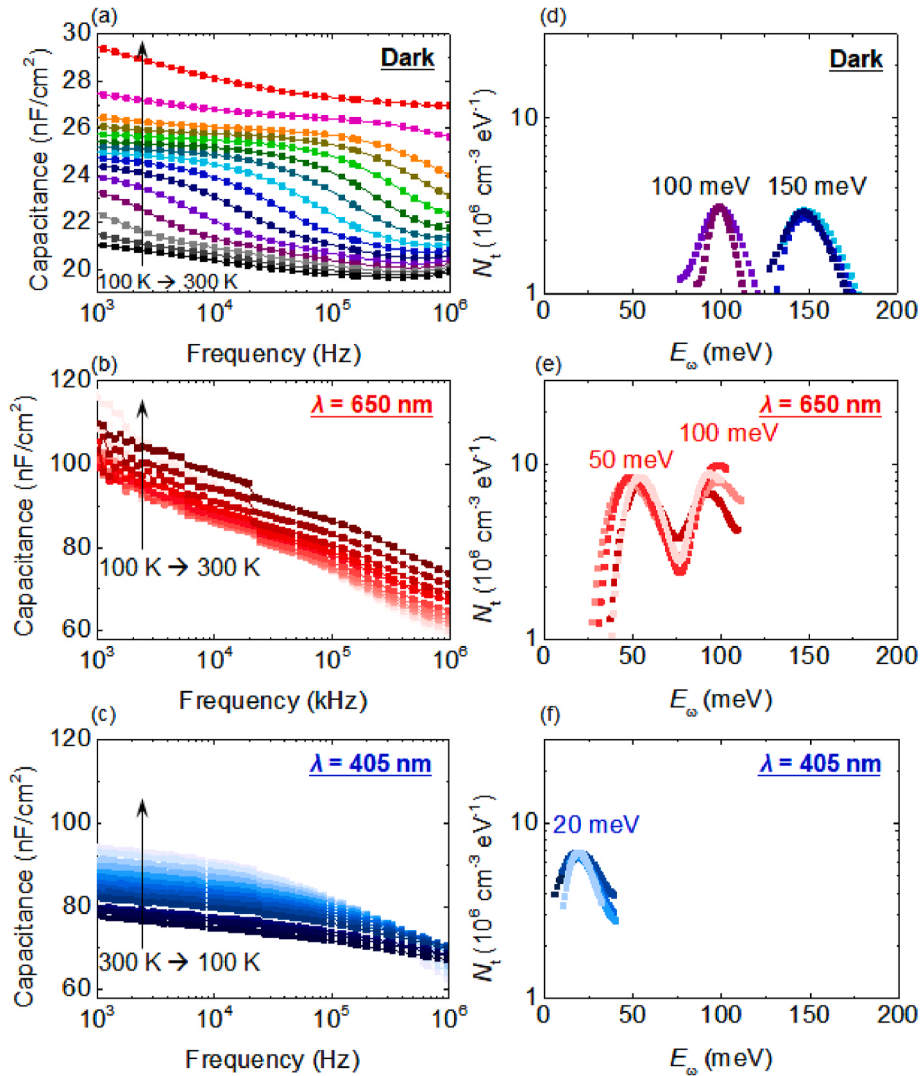


**Fig. 5.** (a, b, c) AS results and (d, e, f) the density of defect states in the dark and under 650 and 405 nm light.

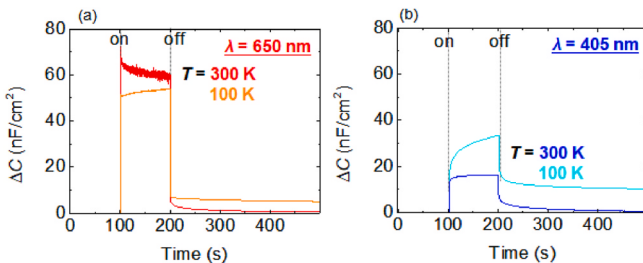


**Fig. 6.** Time dependence of the photo-capacitance for the different illuminations (a) 650 and (b) 405 nm wavelength and temperatures (300 and 100 K).

**Table 3**

Change of photo-capacitance with light on/off and relaxation time with illumination and temperature.

Wavelength (nm)	Temperature (K)	ΔC (nF/cm <sup>2</sup> )	τ <sub>1</sub> (s)	τ <sub>2</sub> (s)
405	100	33	9	157
	300	16	4	122
650	100	54	8	90
	300	59	5	97

illumination than red illumination. The relaxation of the photo-capacitance is well fitted by two exponential components, in accordance with Eq. (10):

$$C(t) = C_{1*} \exp\left(-\frac{t}{\tau_1}\right) + C_{2*} \exp\left(-\frac{t}{\tau_2}\right) \quad (10)$$

where  $C_{1,2*}$  are the pre-exponential factors,  $t$  is time, and  $\tau_{1,2}$  are the time constants of the relaxation. The initially decreasing persistent signal is similarly fast under both illuminations, whereas the decay kinetics for the second relaxation appear slowly under 405 nm light at low temperature. In the turn-on/off dynamics, fast initial rise and fast decay of the photo-capacitance under 650 nm light are associated with the recombination process discussed above. The slow rise and slow decay of the photo-capacitance under the 405 nm illumination can be explained in terms of carrier trapping, which has also been known to lead to reconstruction of the internal electric field in solar cells [35].

The above transport process of photogenerated charge carriers under 650 and 405 nm illumination was thus revealed as the origin of the persistent properties and was shown to occur in the defect states, as indicated by the AS data in Fig. 5. In addition, these persistent photo-capacitance measurements were used to confirm the reversibility of the sample condition after various perturbations, including temperature and light. The correlation of the J-V distortion and dynamics of the photo-induced defect states with temperature was then investigated.

The influence of illumination and temperature upon the mechanism of charge carrier transport can be explained in terms of the band structure of the CdS/CIGS junction shown in Fig. 7. Here, the  $E_g$  is seen to increase at low temperatures relative to that at room temperature, thus leading to increased carrier freezeout and impeding the carriers from passing the barrier at the CdS/CIGS interface, regardless of whether the device is irradiated with light or not. With the large barrier at the CdS/CIGS interface, this limitation of carrier transport leading to the J-V distortion may be the predominant observation [2]. However, we suggest that 405 nm illumination at the CdS/CIGS interface, including the CdS in part, can induce interface defect states that capture holes. As a result, the build-up of captured charges indicated in Fig. 6 causes the redistribution of the internal electric field. This helps carriers pass the barrier at the CdS/CIGS interface, as shown in Fig. 7. Furthermore, the AS results in Fig. 5 can be explained by the suggested model. Thus, the photo-capacitance increases with decreasing temperature under 405 nm light, which is in contrast to the typical AS results for CIGS solar cells. This can be explained by the AS data under 405 nm illumination, which shows that the photogenerated carriers interact with shallow (20 meV) defect states. At low temperatures, no emission was observed as the photogenerated carriers were captured in the shallow defect states, which contributes to an increased capacitance value. By contrast, although increasing  $E_g$  and freezeout of the photogenerated carriers occur under the 650 nm illumination at low temperature, the carriers actively recombine via the defect states, as indicated in Fig. 6. Hence, carrier transport can be limited under 650 nm illumination because an electric field is not generated at low temperature, which leads to a distortion of the J-V curves. At room temperature, however, the

thermionic energy of the charge carriers is sufficiently high to prevent their hindrance via the unfavorable trapping mechanism, even under 405 nm illumination. This is because, at room temperature, thermally-assisted release of any holes that might be trapped in the shallow defect states induced under 405 nm illumination can occur. Therefore, we propose that J-V distortion occurs at low temperature due to the large barrier at the CdS/CIGS interface, which can be overcome by the strong electric field generated by carrier trapping in shallow defect states generated under 405 nm illumination but is not significantly overcome under 650 nm illumination. The trapping of charge carriers in defect states also displays persistent characteristics, as seen from the results of the carrier dynamics study. The origin of the persistent behavior under short wavelength illumination could be explained by slow trapping and emission of the photogenerated carriers.

#### 4. Conclusions

In the present study, we investigated the transport properties of photo-generated carriers in a CIGS solar cell. The measurements were performed under various illumination conditions, including darkness, AM 1.5G, 650 nm, and 405 nm light. The 405 and 650 nm illuminations were shown to excite electron-hole pairs at the CdS/CIGS interface and in the CIGS bulk, respectively, with distinct photocurrent and capacitance characteristics. The distortion of the J-V curve in the dark and under 650 nm light was shown to disappear when the solar cell was subjected to 405 nm light at low temperature. Additionally, a persistent J-V distortion was observed under sequential 650 and 405 nm illumination. The  $V_{OC}$ -T and spatial distribution obtained by DLCP analysis

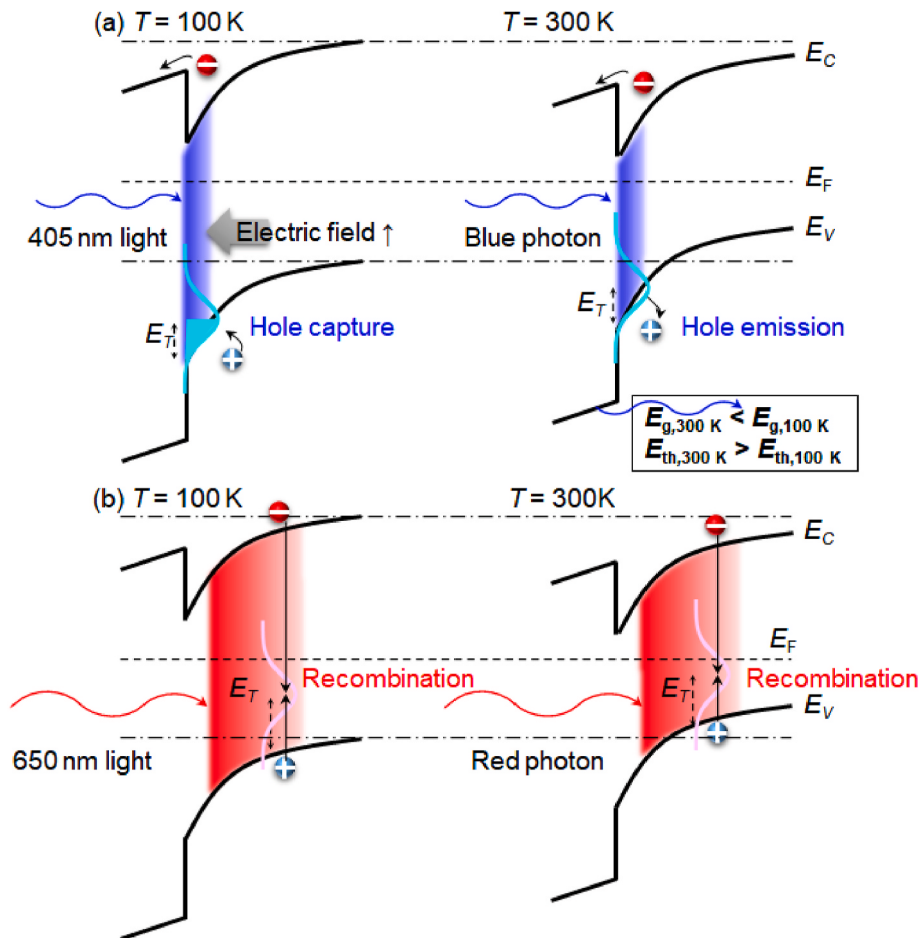


**Fig. 7.** Schematics to explain the illumination wavelength and temperature dependence of carrier transport (a) under blue light and (b) red light. (For interpretation of the references to colour in this figure legend, the reader is referred to the Web version of this article.)

indicated that photogenerated charge carrier transport occurred at the CdS/CIGS interface and was dominant at low temperature. In particular, the carrier dynamics from the frequency- and time-dependent photo-capacitance suggested that shallow defect states induced by the 405 nm light led to a strong electric field that assisted carrier transport at low temperatures. The results suggest that the origin of the *J-V* distortion might be the limitation of charge carrier transport, which can be relieved by the slow trapping of carriers into the blue photon-induced defects; the photons in the blue part of the spectrum also led to the persistent properties of the CIGS solar cells. In addition, we discussed the blue photon-induced shallow defect states and its effect on the band structure, as explained by the thermionic energy. Further, a spectral analysis of the CIGS solar cells demonstrated that the distortion and persistent behaviors observed in the *J-V* curves were influenced by different carrier transport mechanisms under each illumination. The comprehensive analyses in this work provide new interpretation and insight for photon-induced transport behavior and for carrier dynamics as a function of temperature.

#### CRediT authorship contribution statement

**Yunae Cho:** Conceptualization, Investigation, Data Curation, Visualization, Writing - Original Draft. **Jiseon Hwang:** Formal analysis, Investigation, Resources. **Inyoung Jeong:** Methodology, Resources. **Jihye Gwak:** Project administration. **Jae Ho Yun:** Project administration, Funding acquisition. **Kihwan Kim:** Supervision, Methodology, Conceptualization, Validation, Writing - review & editing. **William Jo:** Supervision, Validation, Writing - review & editing.

#### Declaration of competing interest

The authors declare that they have no known competing financial interests or personal relationships that could have appeared to influence the work reported in this paper.

#### Acknowledgements

This research was supported by Basic Science Research Program through the National Research Foundation of Korea (NRF) funded by the Ministry of Education (NRF-2018R1A6A1A03025340), Technology Development Program to Solve Climate Changes of the National Research Foundation of Korea (NRF) funded by the Ministry of Science and ICT (grant no. 2016M1A2A2936753 and 2016M1A2A2936784), and the framework of the Research and Development Program of the Korea Institute of Energy Research (KIER) (CO-2451).

#### Appendix A. Supplementary data

Supplementary data related to this article can be found at <https://doi.org/10.1016/j.solmat.2020.110860>.

#### References

- [1] M.A. Green, E.D. Dunlop, J. Hohl-Ebinger, M. Yoshita, N. Kopidakis, A.W.Y. Ho-Baillie, Solar cell efficiency tables (Version 55), *Prog. Photovoltaics Res. Appl.* 28 (2020) 3–15.
- [2] R. Scheer, H.-W. Schock, Chalcogenide Photovoltaics: Physics, Technologies, and Thin Film Devices, John Wiley & Sons, 2011.
- [3] V. Nadenau, U. Rau, A. Jasenek, H.W. Schock, Electronic properties of CuGaSe<sub>2</sub>-based heterojunction solar cells. Part I. Transport analysis, *J. Appl. Phys.* 87 (2000) 584–593.
- [4] S.S. Hegedus, W.N. Shafarman, Thin-film solar cells: device measurements and analysis, *Prog. Photovoltaics Res. Appl.* 12 (2004) 155–176.
- [5] T. Eisenbarth, T. Unold, R. Caballero, C.A. Kaufmann, H.-W. Schock, Interpretation of admittance, capacitance-voltage, and current-voltage signatures in Cu(In,Ga)Se<sub>2</sub> thin film solar cells, *J. Appl. Phys.* 107 (2010), 034509.
- [6] J.T. Heath, J.D. Cohen, W.N. Shafarman, Bulk and metastable defects in CuIn<sub>1-x</sub>Ga<sub>x</sub>Se<sub>2</sub> thin films using drive-level capacitance profiling, *J. Appl. Phys.* 95 (2004) 1000–1010.
- [7] A. Niemegeers, M. Burgelman, R. Herberholz, U. Rau, D. Hariskos, H.-W. Schock, Model for electronic transport in Cu(In,Ga)Se<sub>2</sub> solar cells, *Prog. Photovoltaics Res. Appl.* 6 (1998) 407–421.
- [8] A. Jasenek, U. Rau, V. Nadenau, H.W. Schock, Electronic properties of CuGaSe<sub>2</sub>-based heterojunction solar cells. Part II. Defect spectroscopy, *J. Appl. Phys.* 87 (2000) 594–602.
- [9] Y. Cho, D.-W. Kim, S. Ahn, D. Nam, H. Cheong, G.Y. Jeong, J. Gwak, J.H. Yun, Recombination in Cu(In,Ga)Se<sub>2</sub> thin-film solar cells containing ordered vacancy compound phases, *Thin Solid Films* 546 (2013) 358–361.
- [10] M. Igelson, M. Bodegård, L. Stolt, Reversible changes of the fill factor in the ZnO/CdS/Cu(In,Ga)Se<sub>2</sub> solar cells, *Sol. Energy Mater. Sol. Cells* 80 (2003) 195–207.
- [11] K. Macielak, M. Maciaszek, M. Igelson, P. Zabierowski, N. Barreau, Persistent photoconductivity in polycrystalline Cu(In,Ga)Se<sub>2</sub> thin films: experiment versus theoretical predictions, *IEEE J. Photovol.* 5 (2015) 1206–1211.
- [12] T. Eisenbarth, R. Caballero, M. Nichterwitz, C.A. Kaufmann, H.-W. Schock, T. Unold, Characterization of metastabilities in Cu(In,Ga)Se<sub>2</sub> thin-film solar cells by capacitance and current-voltage spectroscopy, *J. Appl. Phys.* 110 (2011), 094506.
- [13] I.L. Eisgruber, J.E. Granata, J.R. Sites, J. Hou, J. Kessler, Blue-photon modification of nonstandard diode barrier in CuInSe<sub>2</sub> solar cells, *Sol. Energy Mater. Sol. Cells* 53 (1998) 367–377.
- [14] U. Rau, M. Turcu, A. Jasenek, Time constants of open circuit voltage relaxation in Cu(In,Ga)Se<sub>2</sub> solar cells, *Thin Solid Films* 515 (2007) 6243–6245.
- [15] T. Meyer, F. Engelhardt, J. Parisi, U. Rau, Spectral dependence and Hall effect of persistent photoconductivity in polycrystalline Cu(In,Ga)Se<sub>2</sub> thin films, *J. Appl. Phys.* 91 (2002) 5093–5099.
- [16] A.O. Pudov, J.R. Sites, M.A. Contreras, T. Nakada, H.W. Schock, CIGS J-V distortion in the absence of blue photons, *Thin Solid Films* 480–481 (2005) 273–278.
- [17] T.-M. Cheng, C.-H. Cai, W.-C. Huang, W.-I. Xu, L.-H. Tu, C.-H. Lai, Efficiency enhancement of Cu(In,Ga)(S,Se)<sub>2</sub> solar cells by Indium-doped CdS buffer layers, *ACS Appl. Mater. Interfaces* 12 (2020) 18157–18164.
- [18] F.A. Lindholm, J.G. Fossum, E.L. Burgess, Application of the superposition principle to solar-cell analysis, *IEEE Trans. Electron. Dev.* 26 (1979) 165–171.
- [19] K.-J. Hsiao, J.-D. Liu, H.-H. Hsieh, T.-S. Jiang, Electrical impact of MoSe<sub>2</sub> on CIGS thin-film solar cells, *Phys. Chem. Chem. Phys.* 15 (2013) 18174–18178.
- [20] B. Vermang, V. Fjällstrom, X. Gao, M. Edoff, Improved rear surface passivation of Cu(In,Ga)Se<sub>2</sub> solar cells: a combination of an Al<sub>2</sub>O<sub>3</sub> rear surface passivation layer and nanosized local rear point contacts, *photovoltaics, IEEE J. Photovol.* 4 (2014) 486–492.
- [21] Y. Cho, I. Jeong, M.G. Gang, J.H. Kim, S. Song, Y.-J. Eo, S.K. Ahn, D.H. Shin, J.-S. Cho, J.H. Yun, J. Gwak, K. Kim, Alkali incorporation into Cu(In,Ga)Se<sub>2</sub> determined by crystal orientation of Mo back contact: implications for highly efficient photovoltaic devices, *Sol. Energy Mater. Sol. Cells* 188 (2018) 46–50.
- [22] C.-H. Chung, B. Bob, T.-B. Song, Y. Yang, Current–voltage characteristics of fully solution processed high performance CuIn(S,Se)<sub>2</sub> solar cells: crossover and red kink, *Sol. Energy Mater. Sol. Cells* 120 (2014) 642–646.
- [23] A. Urbaniak, M. Igelson, Creation and relaxation of light- and bias-induced metastabilities in Cu(In,Ga)Se<sub>2</sub>, *J. Appl. Phys.* 106 (2009), 063720.
- [24] M. Igelson, Metastable defect distributions in CIGS solar cells and their impact on device efficiency, *Mater. Res. Soc. Symp. Proc.* 1012 (2007).
- [25] S. Lany, A. Zunger, Light- and bias-induced metastabilities in Cu(In,Ga)Se<sub>2</sub> based solar cells caused by the (V<sub>Se</sub>–V<sub>Cu</sub>) vacancy complex, *J. Appl. Phys.* 100 (2006) 113725.
- [26] D. Redfield, R.H. Bube, Photo-induced Defects in Semiconductors, Cambridge University Press, 2006.
- [27] H.-J. Yu, W.-J. Lee, J.-H. Wi, D.-H. Cho, W.S. Han, Y.-D. Chung, T.-S. Kim, J.-H. Song, Light-soaking effects and capacitance profiling in Cu(In,Ga)Se<sub>2</sub>thin-film solar cells with chemical-bath-deposited ZnS buffer layers, *Phys. Chem. Chem. Phys.* 18 (2016) 33211–33217.
- [28] P. Jackson, R. Wuerz, D. Hariskos, E. Lotter, W. Witte, M. Powalla, Effects of heavy alkali elements in Cu(In,Ga)Se<sub>2</sub> solar cells with efficiencies up to 22.6%, *Phys. PSS RRL* 10 (2016) 583–586.
- [29] S. Minoura, K. Kodera, T. Maekawa, K. Miyazaki, S. Niki, H. Fujiwara, Dielectric function of Cu(In,Ga)Se<sub>2</sub>-based polycrystalline materials, *J. Appl. Phys.* 113 (2013), 063505.
- [30] Z. Wei, C.M. Fung, A. Pockett, T.O. Dunlop, J.D. McGettrick, P.J. Heard, O.J. Guy, M.J. Carnie, J.H. Sullivan, T.M. Watson, Engineering of a Mo/Si<sub>3</sub>N<sub>y</sub> diffusion barrier to reduce the formation of MoS<sub>2</sub> in Cu<sub>2</sub>ZnSnS<sub>4</sub> thin film solar cells, *ACS appl. Energy mater* 1 (2018) 2749–2757.
- [31] R.L. Garris, S. Johnston, J.V. Li, H.L. Guthrey, K. Ramanathan, L.M. Mansfield, Electrical characterization and comparison of CIGS solar cells made with different structures and fabrication techniques, *Sol. Energy Mater. Sol. Cell.* 174 (2018) 77–83.
- [32] M. Cwil, M. Igelson, P. Zabierowski, S. Siebentritt, Charge and doping distributions by capacitance profiling in Cu(In,Ga)Se<sub>2</sub> solar cells, *J. Appl. Phys.* 103 (2008), 063701.
- [33] A.A. Rockett, D.W. Miller, J.D. Cohen, Analysis of CuIn<sub>x</sub>Ga<sub>1-x</sub>Se<sub>2</sub> Solar Cells Using Admittance Spectroscopy Under Light Bias, IEEE Photovoltaic Specialists Conference, 2012, 2012, 001727-001731.

- [34] T. Walter, R. Herberholz, C. Müller, H.W. Schock, Determination of defect distributions from admittance measurements and application to Cu(In,Ga)Se<sub>2</sub> based heterojunctions, *J. Appl. Phys.* 80 (1996) 4411–4420.
- [35] Z. Li, F. Gao, N.C. Greenham, C.R. McNeill, Comparison of the operation of polymer/fullerene, polymer/polymer, and polymer/nanocrystal solar cells: a transient photocurrent and photovoltage study, *Adv. Funct. Mater.* 21 (2011) 1419–1431.
- [36] Z. Li, W. Wang, N.C. Greenham, C.R. McNeill, Influence of nanoparticle shape on charge transport and recombination in polymer/nanocrystal solar cells, *Phys. Chem. Chem. Phys.* 16 (2014) 25684–25693.